Modeling nonstationary spatial data using local likelihood estimation and Matérn-SAR covariance translation

Ashton Wiens[a,*], Douglas Nychka[b], William Kleiber[a]

Colorado, United States

[a]*Department of Applied Mathematics, University of Colorado, Boulder, Colorado, USA*
[b]*Department of Applied Mathematics and Statistics, Colorado School of Mines, Golden, Colorado, USA*

Abstract

Modeling data with nonstationary covariance structure is important to represent heterogeneity in geophysical and other environmental spatial fields. However, spatial data sets with larger numbers of locations are difficult to handle using standard methods. A multistage approach to modeling nonstationary covariances is presented that is efficient for large data sets. The key idea is to divide the modeling into two steps first estimate spatial varying covariance parameters using a local likelihood applied to a moving spatial window. These parameters are then translated into an equivalent model as a spatial autorgression (SAR), that is global and sparse. The global feature of the SAR is a solution to the problem of how to combine the local estimates of the covariance into a single coherent description of a Gaussian process. Moreover, This strategy combines the ease and interpretability of the Matern family of covariances and the efficient computation afforded by spatial models where the precision matrix is sparse. A main result is establishing the accuracy of approximating the Matern family of covariances with a SAR. Also we demonstrate through a Monte Carlo study that local likelihood estimates are accurate even for correlation ranges much larger than the window size provided a sufficient number of replicate fields are available. This has important practical implications for keeping window sizes moderate. The method is applied to an important suite of climate model simulations where replicated fields are available and the covariance varies significantly as the result of land/ocean effects. Although this

[☆]This document is a collaborative effort. Declarations of interest for all authors: none

[*]Corresponding author: Department of Applied Mathematics, University of Colorado, 1111 Engineering Dr, Boulder, CO 80309

Email addresses: ashton.wiens@colorado.edu (Ashton Wiens), nychka@mines.edu (Douglas Nychka), william.kleiber@colorado.edu (William Kleiber)

example benefits from spatial observations on a regular grid the methods are easily extended to irregular data using a basis expansion.

Keywords: nonstationary Gaussian process, local likelihood, Gaussian Markov random field, spatial autoregression, process convolution

1. Introduction

This work is motivated by a climatological application where the goal is to emulate the variability of an ensemble of spatial fields generated by a climate forecast model. Accordingly, we are lead to model spatial data consisting of independent replicated spatial fields that exhibit a nonstationary covariance structure using a Gaussian process. To accurately emulate these fields, modeling the nonstationarity in the second-order structure of the data is essential. To avoid the computation limitations of representing and simulating nonstationary Gaussian processes we investigate a two step approach similar to the methodology in [24]. First, assuming the field is approximately locally stationary, we perform moving window local likelihood estimation to infer spatially varying Matérn covariance parameters. These parameter fields are translated into the parameters of a spatial autoregressive model which best reproduces the behavior of the Matérn correlations locally. Finally, the spatially varying parameters are encoded into the nonstationary SAR covariance model, specifying all of the data jointly.

Local estimation is not a new idea in spatial statistics [11, 12, 33, 29]. A local estimation approach circumvents the $\mathcal{O}(n^3)$ computational burden, where n is the number of observations. Instead, the task becomes n embarrassingly parallel subproblems on the order of the window size used in the local estimation.

We assume that local estimation is a data-driven approach: when the data consists of densely observed independent replicates, robust local estimation of covariance parameters is possible. In practice, there is often no clear indication of which parameters in the model should be allowed to vary spatially [10] and what spatial scales are appropriate for the parameter surfaces. This difficult modeling choice is avoided when using local estimation: we can allow all parameters to vary initially, and the local estimates will indicate whether the parameters are constant or vary over space. Furthermore, with local estimation, we do not have to decompose the parameter functions into some prespecified low-dimensional representation [9, 28], which can influence the estimation.

Weighted local likelihoods have been studied to accommodate irregularly spaced observations [2], but in this work we use a simple moving window applied to data on a lattice. Here, we focus on estimation of Matérn parameters, primarily because of their interpretability and in order to study the relationship between the Matérn and SAR covariance models, detailed below. To establish

local estimation as a reliable technique, we use a Monte Carlo experiment to study the robustness of local estimation of the correlation range parameter.

With locally estimated covariance parameters in hand, some care is required to combine these into a valid global nonstationary covariance model. A simple option is to use the estimates to construct local covariance functions and perform local simulation. However, a global covariance specifying the relationships among all of the data is desirable for efficient simulation and necessary for prediction. A global representation also avoids potential artifacts and ad hoc choices in synthesizing the spatial analysis across local windows.

There are several general classes of nonstationary models, such as deformation methods [31, 3], basis function methods [5, 17, 23, 25], process-convolution construction [14, 16, 15, 26, 8, 7, 35], and the SPDE approach [21, 20, 32, 30]. See [28] for a review of nonstationary models and [13] for a review of methods for large spatial data sets. Unfortunately, only a few of these methods are easily implemented due to the complexity of the models. Here, we investigate two existing nonstationary models from the process convolution and GMRF families of methods which are amenable to plug-in local estimates.

In this work, we study the nonstationary spatial autoregressive (SAR) model, related to the Gaussian Markov random field (GMRF) approach to approximating GPs. The idea is to identify members of the Matérn family of spatial processes as solutions to a stochastic partial differential equation. The SPDE is then discretized to a lattice and this motivates the form of the SAR [21]. The correspondence between the Matérn/SPDE form and a SAR was presented in [21] and an analytical formula was proposed to connect the parameters between the continuous and discrete cases. We have found that the analytical formula is inaccurate for large correlation ranges and one contribution of this work is to sharpen this relationship using numerical results. The advantage is that if one can successfully translate the Matérn formulation into a SAR framework, one can exploit sparse matrix algorithms for fast computation.

Finally, we apply this multistage modeling framework to analyze a nonstationary climate model output data set consisting of 30 temperature anomaly fields from the NCAR CESM project. First, we locally estimate stationary, anisotropic Matérn parameters. We then translate these local Matérn parameters into the SAR parameters which yield the best numerical approximation between the stationary Matérn and the approximately stationary SAR model. Finally, we encode the spatially varying SAR parameters into the nonstationary SAR model. This model convincingly captures many of the nonstationary features of the climate distribution in simulations.

The paper is organized as follows. In section 2, the Matérn family of correlation functions and the process convolution model are introduced, along with the approximately stationary and nonstationary SAR models from the SPDE ap-

proach. We also include a numerical experiment investigating the link between the stationary Matérn and SAR covariance models. In section 3, we develop the local likelihood framework we employ, and we conduct a local estimation simulation study. In section 4, we apply the multistage modeling framework to analyze a nonstationary climatological data set. We conclude with a summary of the method and a discussion of some of the relevant practical aspects.

2. Nonstationary covariance models

In this section, we introduce the Matérn family of covariance models, as well as the process convolution and the SAR/SPDE approaches to constructing a Gaussian process/GMRF. We then state the connection between the Matérn and SPDE models, and explore this relationship in a numerical study.

2.1. The Matérn covariance model

Let $g(\boldsymbol{f})$ be a Gaussian process with mean zero and covariance function $k(\boldsymbol{x}, \boldsymbol{x}')$. The Matérn family of stationary covariance models is important because of its flexibility and the interpretability of its parameters. The Matérn covariance function with a unit range (scale) parameter is

$$k(\boldsymbol{x}, \boldsymbol{x}') = C(\, d \,|\, \nu, \sigma^2 \,) = \sigma^2 \frac{2^{1-\nu}}{\Gamma(\nu)} (d)^{\nu} \mathcal{K}_{\nu}(d)$$

where d is a Euclidean distance between $\boldsymbol{x}$ and $\boldsymbol{x}'$, $\mathcal{K}_{\nu}(\cdot)$ is the modified Bessel function of the second kind of order ν and $\Gamma(\cdot)$ is the gamma function. σ^2 is the spatial process variance (sill), a is the multiplicative range parameter, and ν is the smoothness parameter which controls the mean square differentiability of the process.

This model can be extended to include geometric anisotropy through the definition of the distance that is a linear scaling and rotation of the coordinates. Let $A = D^{-1}U^T$ be a 2×2 matrix where U is a rotation matrix parameterized by angle θ

$$U = \begin{bmatrix} \cos(\theta) & -\sin(\theta) \\ \sin(\theta) & \cos(\theta) \end{bmatrix}$$

and

$$D = \begin{bmatrix} \xi_x & 0 \\ 0 & \xi_y \end{bmatrix}$$

is a diagonal matrix scaling the x and y coordinate axes separately applied. Then the pairwise Mahalanobis distances among the observation locations is defined as $d = \|A\boldsymbol{s} - A\boldsymbol{s}'\|$ and these distances are then used as input to the Matérn covariance function. With this notation we recover an isotropic covariance function setting $\theta = 0$ and $\xi_x = \xi_y$, denoting this common scalar as ξ.

2.2. Process convolution construction

Process convolution is a useful method for constructing valid nonstationary GPs using a spatially varying kernels. Let $\Psi(\boldsymbol{u}, \boldsymbol{v})$ be a kernel with

$$\int_{G\times G} |\Psi(u,v)|^2 d\boldsymbol{u}d\boldsymbol{v} < \infty$$

then we have the process representation

$$Y(\mathbf{s}) = \int_G \Psi(\mathbf{s},\mathbf{u})\,\mathrm{d}W(\mathbf{u})$$

where W is d-variate Brownian motion. It follows that Y has covariance function

$$k(\boldsymbol{s},\boldsymbol{s}') = \int_G \Psi(\boldsymbol{s},\boldsymbol{u})\Psi(\boldsymbol{s}',\boldsymbol{u})d\boldsymbol{u} \tag{1}$$

The advantage of this convolution representation is that any choice of Ψ will yield a valid covariance function and this provides flexibility in devising dependence that varies over the spatial domain. However, except in some special cases the covariance in (1) is difficult to compute in closed form from. To our knowledge only a Gaussian kernel (refHigdon?? is amenable to close form covariance function. Given that parameter estimation and simulation require many evaluations of the covariance at pairs of locations the direct use of this model is problematic. A key idea in this work is that shifting to a SAR process model i that can approximation to this convolution form but also is efficient to evaluate. This is due to a SAR giving rise to sparse precision matrices that approximate the inverses of the covariance matrices.

We note that Paciorek and Schervish [26] have also proposed a family of nonstationary covariance functions. However, this construction deviates from the process convolution approach and since it is in terms of covariances does not result in sparse matrices. it is an open question whether the SAR will approximate the form proposed by Paciorek.

2.3. The SAR model

In contrast to modeling a continuous covariance function, the SAR model parameterizes the precision matrix for the process on a discrete lattice. In our case, we have observations of a spatial field $\mathbf{y}$ located on a regular rectangular grid. This is the setup used throughout the paper and in the data analysis section. We do not believe that this assumption ins overly restrictive for development of this model and in the discussion we explain how to generalize this model to irregularly spaced observations and other linear functionals of the process.

In two dimensions assume the spatial process is indexed as $\boldsymbol{Y}_{i,j}$ and without loss of generality take the integers $1 \leq i \leq m$ and $1 \leq j \leq n$ to be the lattice locations. The isotropic SAR model can be written using graphical notation as

$$\begin{array}{|c|c|c|} \hline 0 & -1 & 0 \\ \hline -1 & 4+1/\kappa^2 & -1 \\ \hline 0 & -1 & 0 \\ \hline \end{array} \tag{2}$$

Given a $\boldsymbol{e}_{i,j}$ distributed independent N(0,1) we interpret the lattice process to satisify

$$(4+\kappa_S^2)\boldsymbol{Y}_{ij} - (\boldsymbol{Y}_{i-1,j} + \boldsymbol{Y}_{i+1,j} + \boldsymbol{Y}_{i,j-1} + \boldsymbol{Y}_{i,j+1}) = e_{i,j}$$

With lattice values outside the range of the indices set to zero.

Here $\kappa_S > 0$ is suggestive of a range parameter controlling the dependence of the field and is similar, although not identical, to κ for the continuous case. For this finite lattice one can identify a matrix, B, Such that $B\boldsymbol{y} = \boldsymbol{e}$ and with $\kappa_S > 0$, B will be invertible. With $\boldsymbol{y} = B^{-1}\boldsymbol{e}$ the covariance matrix for $\boldsymbol{y}$ is $B^{-1}B^{-T}$ and has precision matrix $Q = B^T B$. The precision matrix implied by the SAR model is sparse but in two (or more) dimensions is not banded. The sparsity property makes the SAR model amenable to modeling large data sets because the precision matrix can be used instead of a dense covariance matrix for likelihood estimation and simulation. Following the ideas from refLingrenRue one can iterate the spatial autoregressive weights to obtain higher order models. For example $BB\boldsymbol{y} = \boldsymbol{e}$ impling a SAR extending to second order nearest neighbors has the precision matrix: $Q_2 = (BB)^T(BB)$. The SAR model detailed here is a special case of a Gaussian Markov random field. For a given row of the precision matrix the nonzero, off digaonal entries index the neighbors that will determine the Markov property. Conditioning on these neighbors, the field at a lattice location will be independent of the remaining values of the field. For the first order SAR described above the nonzero elements in Q will include second order neighbors. Thus this first order SAR will be a GMRF based on second order neighbors and the weights will depend on B.

Two additional points should be mentioned about the SAR model. First, this stencil should be modified at the boundaries of the domain. The center value of the stencil should be the κ^2 plus the sum of the weights of its non-zero neighbors. Second, the value of κ affects the marginal variance of the process, so σ^2 is a parameter that allows for modulation of the variance, but it is not the marginal variance of the process itself.

A version of the SAR model that exhibits approximate stationarity and geometrically anisotropic will be detailed in the next section.

2.4. Connection to Matern family

Lindgren, Rue, and Lindström [21] suggested that the SAR covariance model can be thought of as a discrete approximation to the Matérn covariance model. The idea is that a Gaussian Markov random field with SAR covariance can provide an approximation to a Gaussian field with Matérn covariance. The connection is established through an SPDE formulation. In particular, it is known that a Gaussian field $u(\mathbf{s})$ with stationary Matérn covariance is a solution to the SPDE

$$(\kappa^2 - \Delta)^{\alpha/2} u(\mathbf{s}) = \mathcal{W}(\mathbf{s})$$

where $\alpha = \nu + \frac{d}{2}$, $\kappa > 0, \nu > 0$, $\mathbf{s} \in \Omega = \mathbb{R}^d$, $d = 1$ or 2, and $\mathcal{W}(s) \sim \mathrm{WN}(0, \sigma^2)$. As in the Matérn model, ν controls the smoothness of the Gaussian field. Fixing $\nu = 1$ and $d = 2$, the authors showed that the SAR covariance structure obtained by discretizing the pseudodifferential operator $(\kappa^2 - \Delta)$ approximates a Matérn covariance structure with range $a \approx \kappa$.

Similar results can be obtained for different smoothness parameters ν by convolving the finite difference stencil in (2) with itself ν times, as detailed in the previous section for $\nu = 1$ and $\nu = 2$.

This formulation also shows how to extend the SAR model to incorporate geometric anisotropy by including an anisotropy matrix, H, in the Laplacian in the pseudodifferential operator.

$$(\kappa^2 - \nabla \cdot H\nabla)^{\alpha/2} u(\mathbf{s}) = \mathcal{W}(\mathbf{s}) \tag{3}$$

here H is assumed to be symmetric, positive definite. To avoid potential ambiguity we also identify the differential operator above for two dimensions in an expanded form as

$$\nabla \cdot H\nabla \equiv \frac{\partial^2}{\partial^2 s_1} H_{1,1} + 2\frac{\partial^2}{\partial s_1 \partial s_2} H_{2,1} + \frac{\partial^2}{\partial^2 s_2} H_{2,2}$$

Also the first-order finite difference discretization of the anisotropic SPDE gives the following stencil for filling the rows of the B matrix.

$\frac{2H_{12}}{h_x h_y}$	$-\frac{H_{22}}{h_y^2}$	$-\frac{2H_{12}}{h_x h_y}$
$-\frac{H_{11}}{h_x^2}$	$\kappa^2 + \frac{2H_{11}}{h_x^2} + \frac{2H_{22}}{h_y^2}$	$-\frac{H_{11}}{h_x^2}$
$-\frac{2H_{12}}{h_x h_y}$	$-\frac{H_{22}}{h_y^2}$	$\frac{2H_{12}}{h_x h_y}$

(4)

where h_x and h_y are the grid spacings along the x-axis and y-axis. This is just a reparameterization of the results in Appendix A of [21] which facilitates the practical translation of these models. Note that setting $h_x = h_y = 1$ $H_{12} = H_{21} = 0$ and $H_{11} = H_{22} = 1$ one obtains the first order and isotropic model from (2)

Finally we match the role of H in the SPDE formulation to the anisotropic model for the Matern. Under the transformation A=UD from ?? let $\boldsymbol{s}^* = A^{-1}\boldsymbol{s}$ and $u^*(\boldsymbol{s}^*) = u(A\boldsymbol{s}^*)$. Then

$$\nabla u^*(\boldsymbol{s}*) = A(\nabla u)|_{\boldsymbol{s}=A^{-1}\boldsymbol{s}^*}$$

and so we have

$$\nabla \cdot \nabla u = (A\nabla) \cdot A\nabla u^* = (\nabla) \cdot A^T A \nabla u^*.$$

Now identify $H = A^T A$. If the field $u*$ is a solution to (3) then it can also be interpreted as transforming the coordinates of an isotropic field according to A^{-1}. Note that if A is a pure rotation then $H = I$ and isotropy is preserved.

2.5. Numerical translation of range parameters between the Matérn and SAR models

The connection between the anisotropic Matern family and a SAR relies on the approximation of a discretized Laplacian operator with finite differences of the fields on a lattice. To provide an accurate statistical model is important to quantify this approximation and improve its calibration over the limiting expression suggested in [21]. In this section we provide numerical evidence to show that an accurte calibration is possible if restricted to ranges of the covariance parameters.

The computational setup as follows. Given a Matérn range parameter a, we estimate the value of κ in the SAR model which gives the best approximation to the Matérn correlation function. We conducted this experiment with the smoothness of the Matérn model fixed at $\nu = 1$ and $\nu = 2$, and with unit marginal variance for all models. The first step is to fix the Matérn range parameter and evaluate a Matérn correlation matrix on the grid. Then, we perform an optimization over κ by encoding it into the SAR precision matrix using (2), inverting and normalizing it to give the implied SAR correlation matrix, and minimizing the distance between these matrices by some measure.

It is known that the SAR covariance model suffers from edge effects. To avoid the interference of edge effects in this optimization , we quantify the difference between the two correlation matrices by only comparing the correlation of the lattice point in the center of the grid for both models. For an $N \times N$ lattice of locations, with N odd, let σ_a denote the vector of correlations between

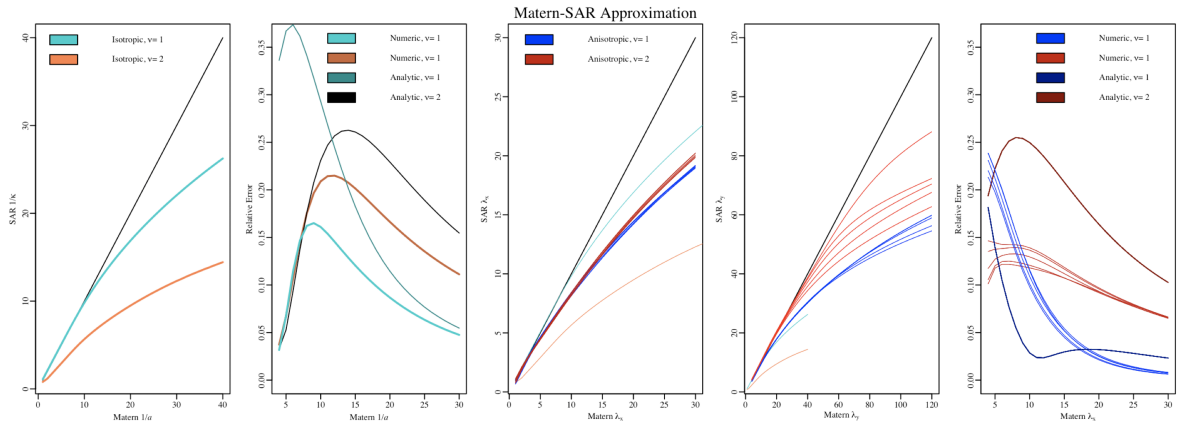

Figure 1: For the isotropic case, the optimal $1/\kappa$ parameter for a given Matérn inverse range $1/a$ is plotted in (a). The relative error incurred by using the SAR model with optimal κ as an approximation to the Matérn model is shown in (b). For the anisotropic case, the optimal diagonal values of H are plotted against the fixed diagonal values of Σ in panels (c) and (d), and the relative error is shown in (e)

the center point in this lattice and all other locations based on the Matern covariance function. Let σ_κ be the same correlation vector for the SAR model with parameter κ. We then find

$$min_\kappa \|\sigma_a - \sigma_\kappa\|$$

Denote this minimzer $\hat{\kappa}(a)$ and so this value will be a mapping from the range parameter of the Matern family into the SAR model.

The approximation results are summarized in Figure 1. Here a is varied over the interval $[1, 40]$, $N = 73$ and the lattice points have unit spacing. In 1(a) $\hat{\kappa}(a)$ is plotting as a function of a. Orange corresponding to the $\nu = 1$ case and cyan corresponding to $\nu = 2$ and the solid black line shows the theoretical relationship, $\frac{1}{a} = \frac{1}{\kappa}$ from [21]. From these computations we conclude that at this level of discretization it is important not to rely on the analytic formula to translate between a and κ parameters.

Figures 1b) and c) The relative error of using the SAR correlation with κ value derived from the numerical experiment is shown in 1(b). The ℓ_2 distance measure used in the optimization of the model correlation matrices is used to quantify the resulting model error, normalized by the ℓ_2 norm of the row from the Matérn correlation matrix.

To make the Matérn ranges comparable between the model with $\nu = 1$ and $\nu = 2$, we used the decorrelation range as a proxy. Specifically, for each Matérn range and fixing $\nu = 1$, we found the distance at which correlation dropped to 0.05. Then, we found the range of Matérn with smoothness $\nu = 2$ which also

decorrelated to 0.05 at the same distance. Note that for comparison we have plotted the smoothness $\nu = 2$ against the $\nu = 1$ range parameters since they are equivalent in the sense just described.

In the data analysis below, we found it necessary to include geometric anisotropy in the covariance model. For this reason, we also investigated how the presence of geometric anisotropy affects the numerical correspondence established for the isotropic case above. The behavior of the approximation was similar to the isotropic case, requiring smaller diagonal values in the anisotropy matrix H than the diagonal values of Σ (the off-diagonal elements of both were set to 0 without loss of generality).

The anisotropic parameter translation results are shown in panels (c) and (d) of Fig 1, with the relative error of approximation shown in panel (e). We tested the length scale ratio $\lambda_x : \lambda_y = 4{:}1$, which was consistent with estimates in the data analysis. In particular, we let $\lambda_x = 1, \cdots, 30$ and $\lambda_y = 4\lambda_x$. The experiment was repeated for 10 rotation angles between $0°$ and $90°$ with $10°$ spacing. The approximation seems may be slightly affected by the rotation angle and oblateness of the geometric anisotropy, but the effect is negligible in practice. From these results, we have ascertained a numerical translation among the anisotropy parameters. We can use these results to translate locally estimated Matérn range parameters into SAR parameters with better accuracy than the conjectured analytic relationship.

2.6. The nonstationary SAR model

The nonstationary SAR model can be constructed by allowing the parameters κ, H, and σ^2 in the generating SPDE to vary over space. The SPDE becomes

$$(\kappa^2(\mathbf{s}) - \nabla \cdot H(\mathbf{s})\nabla)^{\alpha/2} x(\mathbf{s}) = \mathcal{W}(\mathbf{s})$$

where $\kappa(\mathbf{s}) > 0$, $\mathcal{W}(s) \sim \text{WN}(0, \sigma^2(\mathbf{s}))$, and $\sigma^2(\mathbf{s}) > 0$. Discretizing this equation results in a valid GMRF, but it is unclear what covariance function the SAR approximates in this case.

In practice, one can use the discretization in (4) to fill each row of the precision matrix individually, substituting the values for κ and H corresponding to that row's observation location. This gives a sparse banded precision matrix Q with nonconstant bands. The covariance matrix implied by this precision matrix is nonstationary, and the sparse structure of the precision matrix can still be exploited as in the stationary case.

The process variance can also be allowed to vary in the same way as with the nonstationary Matérn model, but this must be done balancing the effects of κ and H. First $\kappa(\mathbf{s})$ and $H(\mathbf{s})$ must be encoded into the precision matrix. The implied marginal variances can then be computed for each location from the

inverse of the precision matrix, and these variances can be adjusted to match the estimated marginal variance.

3. Local moving window likelihood estimation

3.1. Local estimation strategy

Estimating a nonstationarity model can be challenging due to the increased number of covariance parameters. When enough data is available, however, local estimation can give insight into what type of nonstationarity is present.

Local estimation is usually accompanied by the assumption of approximate local stationarity. For this work, we define local stationarity and the local likelihood estimation technique for a Gaussian process with stationary Matérn covariance as follows. First, divide the region of interest $\mathcal{D}$ into M possibly overlapping subregions $\mathcal{D}_1, \mathcal{D}_2, \cdots, \mathcal{D}_M$. Then under the assumption of approximate local stationarity, we can model the data $\mathbf{y}_i$ within the subregion $\mathcal{D}_i$ using a Gaussian process Y_i defined using the following specification:

$$Y_i(\mathbf{s}) = \mu_i(\mathbf{s}) + Z_i(\mathbf{s}) + \epsilon_i(\mathbf{s}) \tag{5}$$

where $\epsilon_i \sim \text{WN}(0, \tau_i^2)$ is spatial white noise and $Z_i \sim \text{GP}(\mathbf{0}, F_i)$ is a spatially correlated Gaussian process with covariance function $F_i(\nu, a_i, \sigma_i^2)$ parameterized by a stationary Matérn covariance function. Let $G_i = F_i + \tau_i^2$. The Gaussian process likelihood of p replicates $\mathbf{y}_i$ which are flattened into a vector is

$$\log L = -\frac{np}{2}\log 2\pi + \frac{1}{2}\log|G\ |^{-1} - \frac{1}{2}(\mathbf{y}_i - \boldsymbol{\mu}_i)^T G^{-1}(\mathbf{y}_i - \boldsymbol{\mu}_i) \tag{6}$$

where $\boldsymbol{\mu}_i$ is the mean function μ_i evaluated at the locations of $\mathbf{y}_i$, and $\mathbf{G}$ is the covariance matrix for $\mathbf{y}_i$ which is block diagonal with blocks G_i. Without loss of generality assume $\boldsymbol{\mu}_i = \mathbf{0}\ \forall i$.

After partitioning the data, each local likelihood estimation is an embarrassingly parallel task, which makes it a viable strategy for large data sets with the help of many processors. If desired, one can assign the location of the center of the subregion $\mathcal{D}_i$ to the estimated parameters $a_i, \sigma_i^2, \tau_i^2,$, which effectively treats the MLEs as spatial fields that can be inspected and smoothed if necessary.

3.2. Local estimation accuracy of the Matérn range parameter

The natural questions when using local estimation techniques are how large of a window should be used and how many replicates of the spatial data are needed to give accurate results. To answer these questions, we designed a computer experiment testing whether covariance parameters can be accurately estimated when using a subset of data with independent replicates. We focus on the Matérn covariance function in estimation because of its prevalence, flexibility,

Figure 2: Each panel displays the absolute percent error from estimating the Matérn range parameter given a certain number of replicates and a window size (size of grid). Fixed Matérn range parameters one, two, three, and four times the size of the grid were tested, faceted in panels (a)-(d). Thin plate splines were fit using the 100 repeated optimization results, performed at each grid location. The splines were used to predict the surfaces shown. The top row corresponds to $\nu = 1$ and bottom to $\nu = 2$. Note that white indicates $> 50\%$ error

interpretability, and the nice theoretical results that exist concerning estimation of the range and variance parameters [18]. Furthermore, by defining the covariance matrix, the model isn't plagued by the edge effects of the SAR model. The goal is to answer how large of a correlation range can be estimated and to what accuracy, given a number of replicates generated with this range and given a certain window size. Using the generated replicates, we numerically find the MLE for the range and record the error of the estimate.

The design of the computer experiment was chosen for practical considerations rather than a traditional design like Latin hypercube sampling. We chose to examine data generated from models with a Matérn range that is one, two, three, and four times the size of the estimation window used. Window sizes were tested between a 5×5 grid and a 33×33 grid, and we used data sets with the number of replicates between 5 and 60. Thus, we have four grids (window size $\times$ number of replicates) based on how large the range is compared to the window size. For each combination of these three factors, we ran the optimization to find the MLE of the range parameter using the generated replicates. The optimization was repeated 100 times using different replicates to mitigate the effect of the random samples in the estimation error. This experiment was conducted twice with Matérn smoothnesses $\nu = 1, 2$. The quantity of interest is the percent error of the estimate. For each of the 4×2 grids, the 100 observations of percent error per location were used to fit thin plate spline models and predict the surfaces shown in Figure (2) (using `fields::Tps` in `R`).

The thin plate spline surfaces can be used as guidelines to decide how many replicates are necessary and what window size should be used to achieve a specific estimation error tolerance, given something is known about the size of the range to be estimated. These results are encouraging: e.g. only a small number of replicates (> 10) are needed with a window size of > 10 to estimate a range of 10. In the extreme case, a Matérn range four times the size of the window might be estimated to within 10% error if 30 replicates are available and using a window size of 10 or greater. Using these guidelines, we can be more confident that local moving window likelihood estimation is a viable technique if enough data is used.

Figure 3: The results of the moving window likelihood estimation. The sill $\sigma^2(\mathbf{s})$ (a), nugget $\tau^2(\mathbf{s})$ (b), geometric average range $\sqrt{\lambda_x(\mathbf{s})\lambda_y(\mathbf{s})}$ (c), and anisotropy ellipses $\Sigma(\mathbf{s})$ (d)

4. Data analysis

In this section, we implement the methods studied in this paper to analyze a data set clearly exhibiting a nonstationary covariance structure. We first use moving window likelihood estimation to infer spatially varying Matérn parameters. We then translate these into their local SAR covariance parameter equivalents, and we encode the spatially varying SAR parameters into the nonstationary SAR covariance model. This model makes it possible to visualize the resulting nonstationary covariance matrix and efficiently simulate new realizations.

4.1. NCAR LENS Data

The data set from the NCAR CESM Large Ensemble project [19] is comprised of 30 spatial fields that we consider independent replicates of the same distribution due to the nature of climate model experiments run with different initial conditions. Nychka [24] first analyzed these data using the LatticeKrig model, and the original article details the climate science application. Details about the pattern scaling approach to statistical emulation can also be found in [1]. Briefly, each field is a measure of how the local temperature average is affected by a global temperature average increase of one degree Celsius. The data locations are on a 288×192 grid with approximately one degree resolution, covering the entire globe.

To streamline this example, we focus on the subregion encompassing the Americas and surrounding oceans containing $13,052$ observations on a 102×128 grid. The top row of Figure 4 shows the first four sample fields from the data set we analyze. The one data modification from [24] is that, in addition to demeaning each grid box, we have also studentized the fields by dividing by the empirical standard deviation of each grid box over the 30 replicates.

4.2. Estimation

First, we performed moving window likelihood estimation as specified in equations (5) and (6). We tested several window sizes between 8×8 and 15×15, and saw little change in the estimates. Based on this range, an 11×11 window size was chosen. This window size is consistent with the long range correlations over the ocean and also the estimate from Section 3.2. The estimation was performed on the NCAR Cheyenne supercomputer [4] using the R programming language [27] with the `Rmpi` [34] and `fields` packages [6]. The details of the

Figure 4: The top row consists of the first four ensemble members from the NCAR CESM data set. The bottom row shows four unconditional simulations from the nonstationary SAR model

Figure 5: Correlations (top) and discrete approximate kernels (bottom) for four locations implied by the nonstationary Matérn model. Note that the bottom row and far right column are at different resolutions

parallel implementation are the same as in [24]. Since the fields were studentized to begin with in this example, we included the constraint $\sigma^2 = 1 - \tau^2$.

The estimates for the spatially varying parameters are shown in Figure 3. The sill and nugget variances are shown in (a) and (b). Panel (c) shows the geometric mean of λ_x and λ_y as a measure of the "average range", which agrees with the range in the isotropic case. Finally in panel (d), a sample grid of the estimated anisotropy matrices $\Sigma(\mathbf{s}_i)$ are plotted by computing the 15% coverage of the bivariate Gaussian covariance ellipses using the `ellipse` package in R [22].

The large signal to noise ratio σ^2/τ^2 (not shown) and the evident transition in the covariance structure between land and ocean indicates that the nonstationarity in the second-order structure of the data is being accurately estimated. Based on the coastlines in some regions, we think that global estimation using some low-dimensional representations of the parameter fields could significantly influence the results; however, the decision is often application specific.

4.3. Using local estimates

The nonstationary SAR model is convenient for plugging in locally estimated parameters and capable of modeling large data sets. For this reason, we chose to translate the local Matérn parameters into their approximate SAR parameter equivalents. The translation was done using the numerical relationship derived in this 2.5. Then, the local SAR parameters were encoded into the nonstationary SAR model. Simulations from this covariance are shown in the bottom row of Figure 4. The simulations do a reasonable job emulating the data, but are lacking some of the long range anisotropy over the ocean.

To gain insight into how the nonstationary SAR model is related to the process convolution construction, we inspect the SAR model's correlations corresponding to individual observation locations, encoded in the rows of the correlation matrix, in the top row of Figure 5. Similarly, plotted in the bottom row of Figure 5 are the rows of the symmetric square root of the correlation matrix, which give a discrete approximation to the kernels that could be used to "construct" the process via the process convolution approach, analogous to $\Psi_{\mathbf{s}}$.

Both anisotropy and nonstationarity are evident in Figure 5. Note the discontinuity off the eastern coast of South America in the discrete approximate

Figure 6: A decorrelated field corresponding to one of the spatial replicates in the data. The precision matrix B applied to the data should result in white noise if the model captures the spatial distribution of the data.

kernel in the third column of the bottom row. This behavior is smoothed out and not seen in the corresponding correlation in the top row.

Finally, in Figure 6 one can see the result of B, the symmetric square root of the precision matrix, applied to one of the replicates to which the model was fitted. To carry out this matrix multiplication, the spatial field is flattened into a vector in the same order specified by the covariance matrix. We used this diagnostic tool to visually assess the goodness of fit of the model covariance matrix to the spatial distribution of the data. If the spatial distribution of the data is fitted correctly, this process should result in a decorrelated field of white noise. Excluding the slight heteroskedasticity present near coastal regions, Figure 6 indicates that the vast majority of the correlation in the data has been captured in the model, and therefore has been removed from the data via this matrix transformation. We did not implement any formal whitening test on the decorrelated fields, although this could be used as a more general goodness of fit test in covariance modeling.

5. Conclusion

In this paper, we have investigated the multistage framework of local estimation and global encoding. We have shown that when independent replicates of approximately locally stationary spatial data are available, robust local estimation is a viable technique for estimating the nonstationarity in the covariance parameters.

We also explored the stationary Matérn-SAR covariance model approximation, conducting a numerical experiment to compare against existing results. It seems that the analytic approximation between the models is not exact for long correlation ranges, and we can use these numerical results to translate parameters between the Matérn and SAR models more accurately.

An important contribution of this work is showing nonstationary data can be modeled by combining local maximum likelihood estimation with a simple global nonstationary covariance model that is straightforward to implement. We focused on encoding the locally estimated parameters in the nonstationary SAR model. In addition, the multistage approach is computationally efficient and can be applied to very large spatial data sets: local estimation avoids the big n problem of global estimation, and encoding local estimates in a SAR model allows us to use sparsity for prediction and simulation. Another major advantage of this method is that it can be applied to both continuously indexed

and lattice data. Local estimation of Matérn parameters can incorporate regular or irregularly spaced data, and can always be performed in a way that makes encoding in the discrete SAR model possible.

[1] Alexeeff, S. E., Nychka, D., Sain, S. R., Tebaldi, C., 2018. Emulating mean patterns and variability of temperature across and within scenarios in anthropogenic climate change experiments. Climatic Change 146 (3-4), 319–333.

[2] Anderes, E. B., Stein, M. L., 2011. Local likelihood estimation for nonstationary random fields. Journal of Multivariate Analysis 102 (3), 506–520.

[3] Anderes, E. B., Stein, M. L., et al., 2008. Estimating deformations of isotropic gaussian random fields on the plane. The Annals of Statistics 36 (2), 719–741.

[4] Computational and Information Systems Laboratory, 2017. Cheyenne: HPE/SGI ICE XA System (University Community Computing).

[5] Cressie, N., Johannesson, G., 2008. Fixed rank kriging for very large spatial data sets. Journal of the Royal Statistical Society: Series B (Statistical Methodology) 70 (1), 209–226.

[6] Douglas Nychka, Reinhard Furrer, John Paige, Stephan Sain, 2017. fields: Tools for spatial data. R package version 9.6.
URL `www.image.ucar.edu/~nychka/Fields`

[7] Fuentes, M., 2002. Spectral methods for nonstationary spatial processes. Biometrika 89 (1), 197–210.

[8] Fuentes, M., Smith, R. L., 2001. A new class of nonstationary spatial models. Tech. rep., Technical report, North Carolina State University, Raleigh, NC.

[9] Fuglstad, G.-A., Lindgren, F., Simpson, D., Rue, H., 2015. Exploring a new class of non-stationary spatial gaussian random fields with varying local anisotropy. Statistica Sinica, 115–133.

[10] Fuglstad, G.-A., Simpson, D., Lindgren, F., Rue, H., 2015. Does non-stationary spatial data always require non-stationary random fields? Spatial Statistics 14, 505–531.

[11] Haas, T. C., 1990. Kriging and automated variogram modeling within a moving window. Atmospheric Environment. Part A. General Topics 24 (7), 1759–1769.

[12] Haas, T. C., 1990. Lognormal and moving window methods of estimating acid deposition. Journal of the American Statistical Association 85 (412), 950–963.

[13] Heaton, M. J., Datta, A., Finley, A., Furrer, R., Guhaniyogi, R., Gerber, F., Gramacy, R. B., Hammerling, D., Katzfuss, M., Lindgren, F., et al., 2017. Methods for analyzing large spatial data: A review and comparison. arXiv preprint arXiv:1710.05013.

[14] Higdon, D., 1998. A process-convolution approach to modelling temperatures in the north atlantic ocean. Environmental and Ecological Statistics 5 (2), 173–190.

[15] Higdon, D., 2002. Space and space-time modeling using process convolutions. In: Quantitative methods for current environmental issues. Springer, pp. 37–56.

[16] Higdon, D., Swall, J., Kern, J., 1999. Non-stationary spatial modeling. Bayesian statistics 6 (1), 761–768.

[17] Katzfuss, M., Cressie, N., 2011. Spatio-temporal smoothing and em estimation for massive remote-sensing data sets. Journal of Time Series Analysis 32 (4), 430–446.

[18] Kaufman, C., Shaby, B., 2013. The role of the range parameter for estimation and prediction in geostatistics. Biometrika 100 (2), 473–484.

[19] Kay, J., Deser, C., Phillips, A., Mai, A., Hannay, C., Strand, G., Arblaster, J., Bates, S., Danabasoglu, G., Edwards, J., et al., 2015. The Community Earth System Model (CESM) large ensemble project: A community resource for studying climate change in the presence of internal climate variability. Bulletin of the American Meteorological Society 96 (8), 1333–1349.

[20] Lindgren, F., Rue, H., 2007. Explicit construction of gmrf approximations to generalised matérn fields on irregular grids. Preprints in Mathematical Sciences 5.

[21] Lindgren, F., Rue, H., Lindström, J., 2011. An explicit link between gaussian fields and gaussian markov random fields: the stochastic partial differential equation approach. Journal of the Royal Statistical Society: Series B (Statistical Methodology) 73 (4), 423–498.

[22] Murdoch, D., Chow, E. D., 2018. ellipse: Functions for Drawing Ellipses and Ellipse-Like Confidence Regions. R package version 0.4.1.
URL `https://CRAN.R-project.org/package=ellipse`

[23] Nychka, D., Bandyopadhyay, S., Hammerling, D., Lindgren, F., Sain, S., 2015. A multiresolution gaussian process model for the analysis of large spatial datasets. Journal of Computational and Graphical Statistics 24 (2), 579–599.

[24] Nychka, D., Hammerling, D., Krock, M., Wiens, A., 2018. Modeling and emulation of nonstationary gaussian fields. Spatial Statistics.

[25] Nychka, D., Wikle, C., Royle, J. A., 2002. Multiresolution models for nonstationary spatial covariance functions. Statistical Modelling 2 (4), 315–331.

[26] Paciorek, C. J., Schervish, M. J., 2004. Nonstationary covariance functions for gaussian process regression. In: Advances in neural information processing systems. pp. 273–280.

[27] R Core Team, 2018. R: A Language and Environment for Statistical Computing. R Foundation for Statistical Computing, Vienna, Austria.
URL `https://www.R-project.org/`

[28] Risser, M. D., 2016. Nonstationary spatial modeling, with emphasis on process convolution and covariate-driven approaches. arXiv preprint arXiv:1610.02447.

[29] Risser, M. D., Calder, C. A., 2015. Local likelihood estimation for covariance functions with spatially-varying parameters: the convospat package for r. arXiv preprint arXiv:1507.08613.

[30] Rue, H., Held, L., 2005. Gaussian Markov random fields: theory and applications. CRC press.

[31] Sampson, P. D., Guttorp, P., 1992. Nonparametric estimation of nonstationary spatial covariance structure. Journal of the American Statistical Association 87 (417), 108–119.
URL `http://www.jstor.org/stable/2290458`

[32] Simpson, D., Lindgren, F., Rue, H., 2012. Think continuous: Markovian gaussian models in spatial statistics. Spatial Statistics 1, 16–29.

[33] Ver Hoef, J. M., Cressie, N., Barry, R. P., 2004. Flexible spatial models for kriging and cokriging using moving averages and the fast fourier transform (fft). Journal of Computational and Graphical Statistics 13 (2), 265–282.

[34] Yu, H., 2002. Rmpi: parallel statistical computing in R. R News 2 (2), 10–14.

[35] Zhu, Z., Wu, Y., 2010. Estimation and prediction of a class of convolution-based spatial nonstationary models for large spatial data. Journal of Computational and Graphical Statistics 19 (1), 74–95.